



# Enhanced strength–ductility synergy of carbon nanotube/Al–Cu–Mg composites via introducing laminate structure and grain modification

P.Y. Li<sup>a,b</sup>, X.N. Li<sup>b</sup>, Z.Y. Liu<sup>b,\*</sup>, L.Q. Chen<sup>a</sup>, B.L. Xiao<sup>b</sup>, Z.Y. Ma<sup>b</sup>

<sup>a</sup> State Key Laboratory of Rolling and Automation, Northeastern University, 3-11 Wenhua Road, Shenyang, 110819, China

<sup>b</sup> Shi-changxu Innovation Center for Advanced Materials, Institute of Metal Research, Chinese Academy of Science, Shenyang, 110016, China

## ARTICLE INFO

### Keywords:

Carbon nanotubes  
Metal-matrix composite  
Laminate  
Mechanical property

## ABSTRACT

Laminate carbon nanotube (CNT)/Al–Cu–Mg composites consisting of alternate ductile layers (coarse or ultrafine grain Al) free of CNTs and brittle layers (ultrafine grain) rich in CNTs, were prepared in the powder metallurgy route. It was found that the strength–ductility of the composites was improved remarkably, as compared with those of uniform composites. Mechanical incompatibility between different layers during tensile deformation produced a large number of geometrically necessary dislocations (GNDs) between the ductile layers and the brittle layers, which inhibited the strain localization, thereby enhancing the strength–ductility. Compared with the laminate composite using the coarse grain Al as the ductile layers, the strength of the laminate composite using ultrafine grain Al as ductile layers further increased by 14%, while the elongation remained unchanged. This was because the ultrafine grain rather than coarse grain of the ductile layers could lead to higher strength and had better coordination with the brittle layers.

## 1. Introduction

Carbon nanotubes (CNTs) reinforced aluminum (Al) composites have been considered ideal lightweight structural materials that have exceptional mechanical performance [1–3]. In the past decades, CNT showed an extraordinary strengthening effect on the Al matrix, and various strengthening mechanisms have been proposed [4–6]. Unfortunately, owing to the low dislocation storage capability of ultrafine grains (UFGs) and the pinning effect of CNT on dislocation, the strength enhancement of CNT/Al composites is usually accompanied by considerable loss of ductility, which limits their engineering applications [7–11].

Some studies have shown that grain modification by plastic deformation could improve the mechanical properties of Al-based materials [12,13]. However, these methods are difficult to further coarsen grains in CNT/Al due to the presence of CNTs. To overcome the problem of low strength–ductility, heterogeneous structure design has been proved to be a potentially effective method to improve the strength–ductility of UFG metal or ceramic materials [14–17]. To date, some unusual combinations of enhanced strength–ductility have been reported in different heterogeneous systems, including bimodal [17], bio-inspired [18–20], and laminate structure composites [21–23]. E.g. the bimodal

CNT/Al–Cu–Mg composites could be prepared by the powder metallurgy (PM) method combined with subsequent plastic deformation such as hot extrusion [17]. Compared with uniform CNT/Al–Cu–Mg composites, the ductility of bimodal composites increased significantly, while the ultimate tensile strength almost had no loss. The increase in elongation was due to the coarse-grained ductile zone which greatly restrained strain localization and effectively passivated microcracks.

However, the influence of the ductile zone (DZ) morphologies and dispersion on strength–ductility synergy heterogeneous composites are still unclear. As one of the most typical heterogeneous structures, it has been proved that the laminate structures consisting of ductile layers (DLs) and brittle layers (BLs) could achieve an excellent balance of strength and ductility [16,24–32]. For example, the strength–ductility synergy of laminate Ti/Al composite was improved significantly [33]. It should be pointed out that the DZs of bimodal composites were dispersed bands while those of laminate composites were connected. That is, the laminate structure could reflect the morphological and dispersive difference in the DZ.

In addition, the reason for the strength–ductility synergy enhancement of metal laminates was the back stress induced by the deformation mismatch of two metal layers at different tensile stages [33]. However, it was not clear whether the strength–ductility improvement of the

\* Corresponding author.

E-mail address: [zyliu@imr.ac.cn](mailto:zyliu@imr.ac.cn) (Z.Y. Liu).

<https://doi.org/10.1016/j.compositesb.2022.110178>

Received 27 April 2022; Received in revised form 23 July 2022; Accepted 26 July 2022

Available online 1 August 2022

1359-8368/© 2022 Elsevier Ltd. All rights reserved.

laminated CNT/Al composites is the same as that of metal laminates. Therefore, the CNT/Al composite with laminated structure could be used as a model material, to research the tensile behavior of laminated composites.

In this study, CNT/2009Al composites consisting of alternate DLs (2009Al) and BLs (CNT/2009Al) were fabricated by the PM method. The laminated composites with the coarse grain (CG) and ultrafine grain (UFG) DLs were also respectively designed for comparison. The objectives are (a) to develop CNT/Al composites with high strength and high ductility through laminated structure design; (b) to improve the strength-ductility of laminated composites via grain modification in DLs and clarify the tensile behaviors.

## 2. Experimental

### 2.1. Powder preparation

The as-received CNTs with an average diameter of 10 nm, and a length of more than 5  $\mu\text{m}$  (Fig. 1(a)), were provided by Tsinghua University. The atomized 2009Al alloy powders with an average diameter of 10  $\mu\text{m}$  (Fig. 1(b)), had a composition of Al-4.5 wt% Cu-1.5 wt% Mg. The milled 2009Al alloy (Fig. 1(c)) and 3 vol% CNT/2009Al composite (Fig. 1(d)) powders were respectively obtained by ball milling in an attritor running at 250 rpm with a ball-to-powder ratio of 15:1 for 10 h in a purified argon atmosphere. The inset image of Fig. 1(e) indicates that CNTs could be singly inserted into Al powders after milling.

### 2.2. Laminated composite fabrication

The as-atomized and as-milled 2009Al were respectively used to obtain DLs, while the 3 vol% CNT/2009Al powders were used to obtain

BLs for the laminated composites. The schematic of routes for preparing laminated composites is shown in Fig. 2. Firstly, the DL and BL powders were alternately laid into a cylinder die, followed by cold compacted and vacuum hot pressed at 813 K into billets with the layer thickness ratio of 1:2. This thickness ratio could obtain the laminated composite with a nominal CNT concentration of 2 vol%. Cylindrical materials were taken out from the billets perpendicular to the hot-pressing direction, and then hot extruded into bars with an extrusion ratio of 16:1 at 723 K. The hot-extruded bars were further hot-rolled at 753 K along the extrusion direction by several passes to 75% reduction at a ratio of 15% reduction per pass. Finally, the hot-rolled composites were solution treated at 773 K for 2 h, then quenched into the water, and aged naturally for more than 96 h.

For simplification, the CG 2009Al DL-CNT/2009Al BL and UFG 2009Al DL-CNT/2009Al BL laminated composites were abbreviated as CG DL-BL and UFG DL-BL, respectively. For comparison, the 2 vol% CNT/2009Al composite with uniform structure, as well as the corresponding DL and BL materials for the laminated composite, namely CG 2009Al, UFG 2009Al, and 3 vol% CNT/2009Al with the uniform structure were fabricated under the same hot-pressing, rolling, and heat treatment processing.

### 2.3. Microstructure characterization and tensile test

The layer structure and longitudinal section of fracture surface morphology for different laminated composites were observed using an optical microscope (OM; Zeiss Ax overt 200MAT). A field emission scanning electron microscope (FEI, Apreo) was used to characterize the fracture surfaces and powder morphology. The grain structure, dislocation, and CNT distribution in laminated composites were estimated by transmission electron microscopy (FEI, Talos). High-resolution TEM

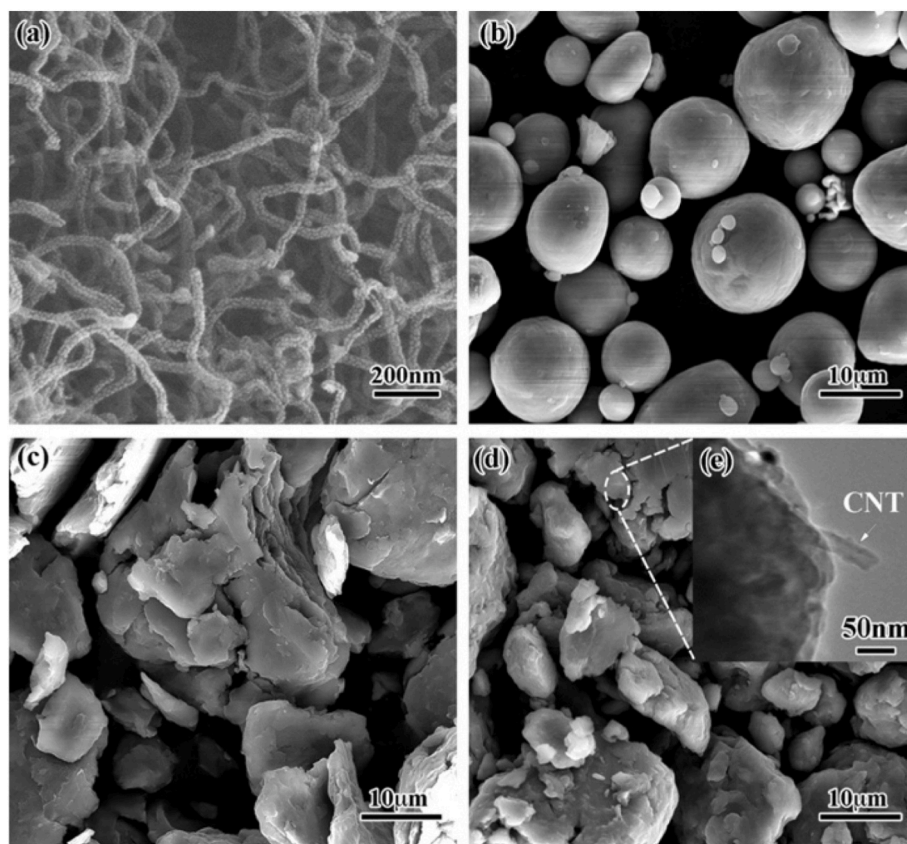


Fig. 1. SEM images of different powders: (a) as received CNT, (b) as atomized 2009Al, (c) as milled 2009Al, and (d) as milled 3 vol% CNT/2009Al (The inset shows CNT distributions in milled composite powders under TEM).

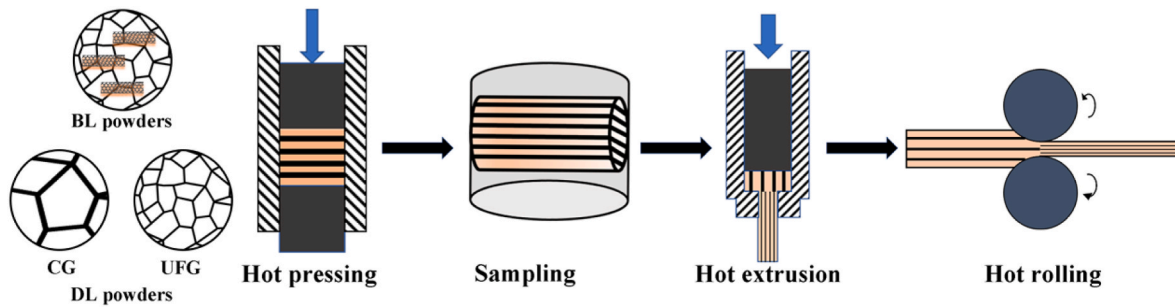


Fig. 2. Schematic of the preparation route for the laminate composites.

(HRTEM) was used to examine the structure of the area around the CNT-Al interface. The grain size was measured by using high-angle annular dark-field (HAADF) images under TEM.

Tensile specimens with a gauge length of 28 mm, a width of 4 mm, and a thickness of 2 mm were machined parallel to the rolled direction from the rolled sheets. Uniaxial tensile tests were carried out to evaluate the mechanical properties using an Instron 5982 tester at an initial strain rate of  $1 \times 10^{-3} \text{ s}^{-1}$  at room temperature. At least three specimens were tested for each material.

### 3. Results

#### 3.1. Microstructure of laminate composites

Fig. 3(a) and (b) show the layer structure of the laminate composites. It can be seen that an obvious alternate structure of white layers and dark layers could be successfully achieved, and the different layers were densely bonded without pore defects. The white and dark layers could respectively be the DLs free of CNTs and BLs rich in CNTs, because of the higher susceptibility of the BLs to chemical etching as a result of the higher fraction of phase boundaries. The average DL and BL thickness of the CG DL-BL were respectively  $66.6 \mu\text{m}$  and  $96.1 \mu\text{m}$  (Fig. 3 (a)), while the average DL and BL thickness of the UFG DL-BL were respectively  $43.1 \mu\text{m}$  and  $85.8 \mu\text{m}$  (Fig. 3 (b)). This indicates that the thickness ratio of DL to BL for the UFG DL-BL was close to the initial ratio of 1:2, while the thickness ratio of DL-BL for the CG DL-BL was about 1:1.5.

No CNTs could be observed in the DLs for either CG DL-BL or UFG

DL-BL, and the grain sizes in the DLs for the CG DL-BL and UFG DL-BL were respectively  $1 \mu\text{m}$  and  $300 \text{ nm}$  (Fig. 3 (c) and (d)). The BLs of both laminate composites had a similar structure. In the BLs, the grain sizes were much fine, about  $200\text{--}300 \text{ nm}$  (Fig. 3(e)). Further, many CNTs could be observed and were singly dispersed in the BLs (Fig. 3(f)). The CNTs were approximately aligned in the rolling direction (Fig. 3 (f)), which is mainly attributed to the pure shear plastic flow during hot-rolling [34].

The microstructure of the DL-BL boundary of the laminate composites is shown in Fig. 4. The TEM and HRTEM images are shown in Fig. 4 (a–f) further verify that no pore defects were observed at the BL-DL boundary and the two layers were densely bonded. The element mapping shown in Fig. 4(f) demonstrates that no element segregation of Cu or Mg could be detected at the BL-DL boundary. All of these demonstrate that the BLs and DLs were relatively independent and well bonded.

The HRTEM images of the structure around the CNT-Al interface in the BLs of the laminate composites are shown in Fig. 5. It indicates that the wall structures of CNTs were well retained and the CNT-Al interfaces were well bonded (Fig. 5(a) and (b)), indicating that the subsequent hot-rolling did not further damage the structures of CNTs. Further, some nano-scale  $\text{Al}_4\text{C}_3$  particles were formed in the area attached to or near some CNTs (Fig. 5(c) and (d)). It is well known that a certain amount of interfacial reaction could increase the interface bonding and was beneficial to enhancing the strengthening efficiency [35–37].

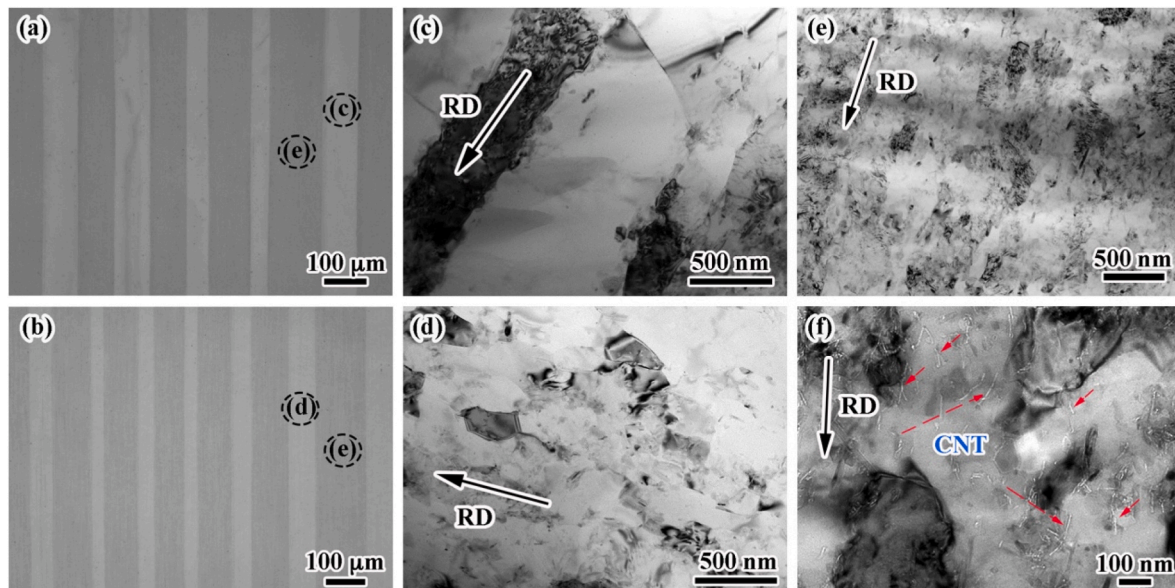


Fig. 3. Layer structure and grain in DL for (a) (c) the CG DL-BL, (b) (d) UFG DL-BL; (e) (f) grain and CNT distribution in BL.

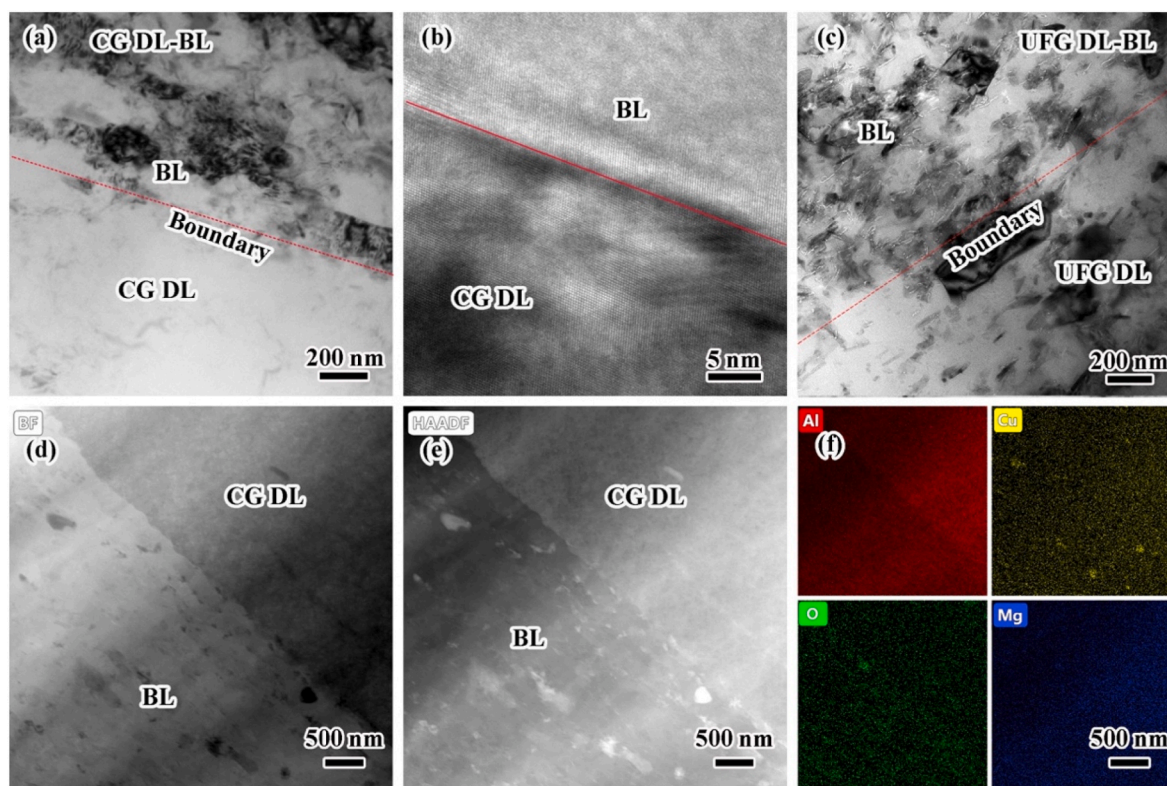


Fig. 4. The TEM and HRTEM images of the laminate composite boundaries between DL and BL in laminate composites: (a) and (b) CG DL-BL, (c) UFG DL-BL, and (d)–(f) BF, HAADF, and the element mapping of CG DL-BL.

### 3.2. Tensile properties of composites

The tensile curves of the laminate composites and their corresponding layer materials are shown in Fig. 6(a), and the yield strength (YS), ultimate tensile strength (UTS), and elongation (El) in detail are listed in Table 1. The CG 2009Al had a relatively low YS (248 MPa) and UTS (446 MPa), but a much higher El of about 20%. In comparison with the CG 2009Al, the UFG 2009Al showed remarkably enhanced YS (540 MPa) and UTS (648 MPa), while it remained at a relatively high El of 10%. By introducing the CNTs, the uniform 3 vol% CNT/2009Al composite showed a much high UTS of about 760 MPa, but a very low El of only 1.6%. Namely, the strength of uniform composites increased but the ductility reduced significantly. Many studies have confirmed that the strengthening mechanisms of uniform composites are mainly fine grain and load transfer strengthening [38,39].

By introducing the CG DL to form the laminate composite (CG DL-BL), the El was pronouncedly increased from 1.6% to 4.8%, however, the YS reduced a lot from 686 MPa to 554 MPa and the UTS reduced from 765 MPa to 660 MPa. By refining the grain size of DL via introducing UFG DL to form the laminate composite (UFG DL-BL), both the UTS and YS increased about 70 MPa, as compared with those of CG DL-BL. It should be mentioned that the El of the UFG DL-BL laminate composite retained the same elongation as that of the CG DL-BL laminate composite.

Fig. 6(b) shows the tensile strain-stress curves of CNT/2009Al composites with nominal 2 vol% CNT, including the uniform and two laminate composites. It can be seen that the El of two laminate composites increased from 3.7% to 4.8%, as compared with that of uniform CNT/2009Al, which indicated that the laminate structure had an obvious effect on improving ductility. For the CG DL-BL laminate composite, the YS reduced by about 11%, and the UTS reduced by 6%, as compared to those of the uniform composite. However, for the UFG DL-BL composite, either the YS or the UTS was even a little higher than those of the uniform composite. This means that the strength and

elongation increase simultaneously by optimizing the grain structure of the BL.

Further, the tensile curve of the uniform composite had an obvious fluctuation. By comparison, the tensile curves for the two laminate composites were much smoother, which also demonstrates that the existence of DL in the laminate structure could coordinate the plastic deformation of BL. This phenomenon was in accordance with the finding reported in bimodal composites [17].

Usually, the energy absorbed per volume of a material can be represented by the strength-ductility combination, which can be further obtained from the area under the strain-stress curve [48]. To simply estimate the area, a strength-ductility product (SDP)  $\sim 0.5(YS + UTS) \times El$  was used to calculate the area [17]. The SDP of laminate composites and the corresponding layer materials were listed in Table 1. For uniform composites, the incorporation of CNTs improved the strength of the composites, but the elongation was considerably reduced. As a result, the SDP of uniform 2 vol% and 3 vol% CNT/2009Al were respectively 24 and 12 MJ/m<sup>3</sup>, much lower than those of CG or UFG 2009Al. By constructing the laminate structure, the SDP value increased by at least 18% to that of the uniform composite. Especially, the SDP of the UFG DL-BL composite was 43% higher than that of the uniform composite. These results demonstrate that using the UFG 2009Al as the DLs of laminate structure could effectively enhance the strength-ductility of the composite.

Fig. 6(c) shows the strength-ductility comparison of CNT/Al composites reported in literatures [2,17,40–47]. It can be seen that all of the composites exhibit a trade-off between strength and ductility, that is, high strength accompanied by low ductility. However, the laminate composites exhibit a relatively higher strength-ductility, as compared with those of the reported uniform composites.

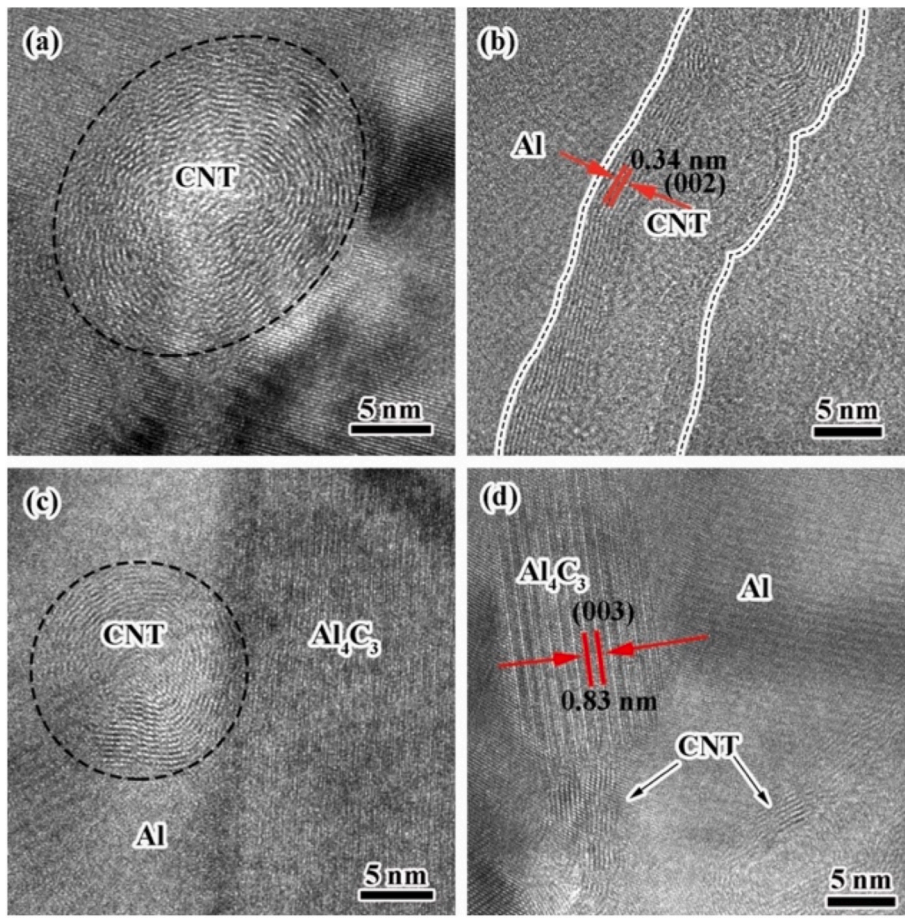


Fig. 5. The HRTEM images of the structure around the CNT-Al interface in the BLs.

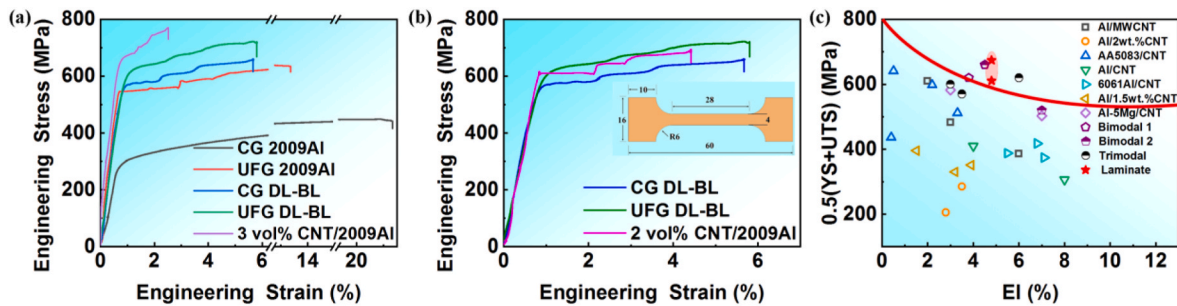


Fig. 6. (a) Tensile curves of the laminate composites and corresponding DL and BL materials, (b) Tensile curves of uniform and laminate CNT/2009Al with nominal 2 vol% CNT, (c) Strength-ductility comparison of CNT/Al composites fabricated by HEBM [2,17,40–47].

Table 1  
Tensile properties of the matrix, uniform composites, and laminate composites.

Sample	YS (MPa)	UTS (MPa)	EI (%)	SDP (MJ/m <sup>3</sup> )
CG 2009Al	284 ± 20	446 ± 8	21.2 ± 0.8	70.4
UFG 2009Al	540 ± 17	648 ± 3	10.6 ± 1.6	63.3
2 vol% CNT/2009Al	624 ± 8	700 ± 5	3.7 ± 1.0	24.8
3 vol% CNT/2009Al	686 ± 10	765 ± 8	1.7 ± 0.2	12.7
CG DL-BL	554 ± 5	660 ± 4	4.8 ± 0.3	29.3
UFG DL-BL	628 ± 3	720 ± 6	4.8 ± 0.2	32.6

#### 4. Discussion

##### 4.1. Effect of the laminate structure on tensile behavior

Fig. 7(a) shows the magnified tensile curves of the uniform and laminate composites. In view of the tensile curve shape, the uniform composite showed an obvious fluctuation in the tensile curve. After introducing the laminate structure, the fluctuation changed much more smoothly. Especially, the UFG DL-BL was even smoother than the CG DL-BL. This indicates the introduction of the DLs could effectively coordinate the deformation of the BLs, and the UFG DLs were more effective due to the smaller grain size difference between BLs and DLs.

Fig. 7(b) shows the strain hardening rate ( $\Theta$ ) for uniform and laminate composites. It can be seen that  $\Theta$  of CG DL-BL and UFG DL-BL decreased rapidly at first in region I, even below zero, and then raised

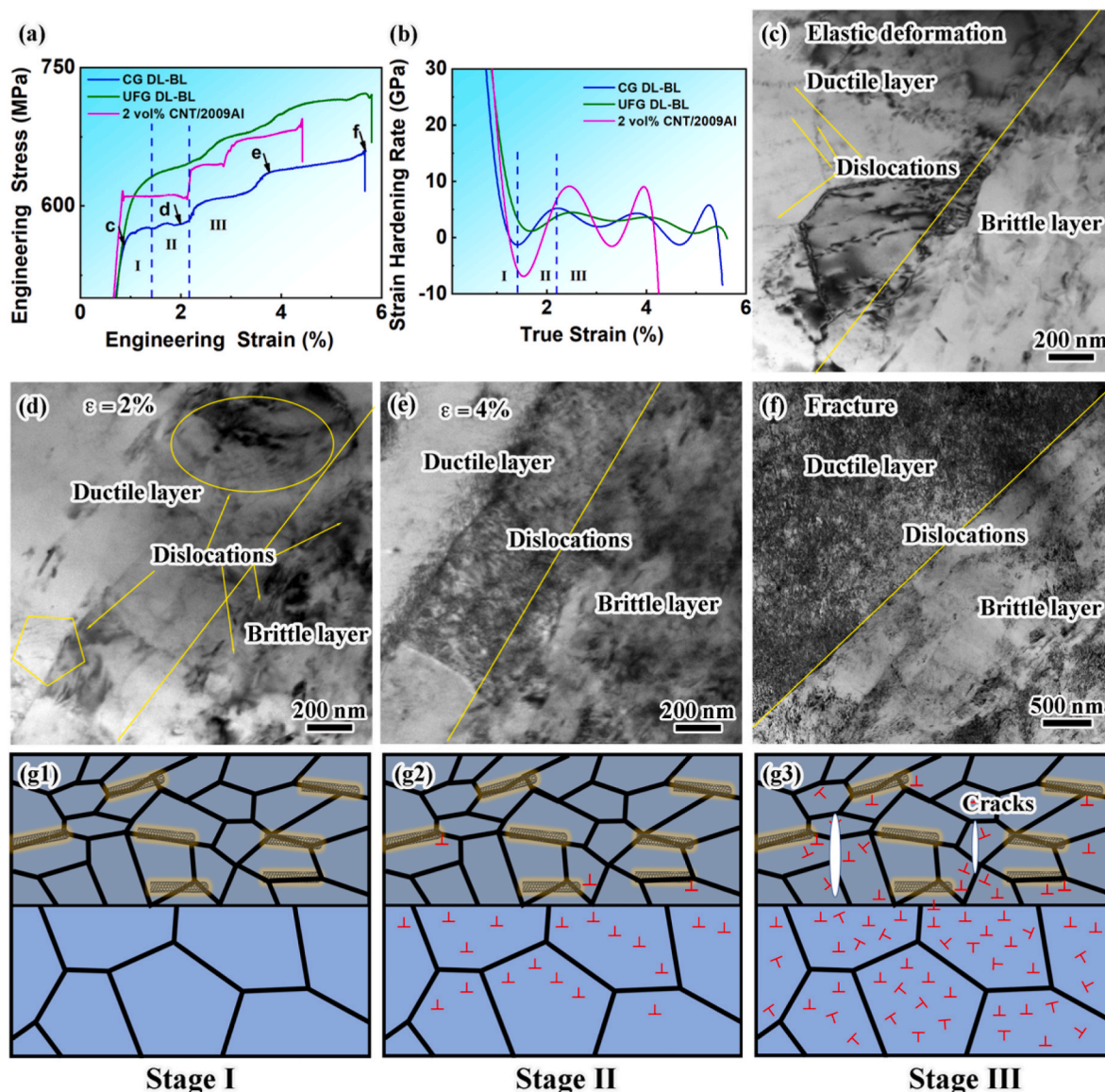


Fig. 7. (a) Locally magnified tensile curves and (b) Strain-hardening of the uniform and laminate composites. (c)–(f) ex-situ TEM images showing the dislocation evolution corresponding to the tip-drop on tensile curves at point “c-f”. (g1)–(g3) Schematic illustration of the dislocation evolution during deformation. Stage I: elastic deformation; Stage II: elastic-plastic deformation; Stage III: plastic deformation.

in region II, reaching their first maximum value, which was a common phenomenon in heterogeneous materials [14,49–51]. This transient behavior could be attributed to the lack of mobile dislocations in BL with UFG, which was difficult to adapt to the constant strain rate applied at the beginning of the plastic deformation in region I [14]. After yielding, the proliferation and entanglement of dislocations resulted in a rapid increase  $\Theta$  in region II [14]. The curves show that the CG DL-BL sample maintained relatively high  $\Theta$  during the tensile deformation, even slightly higher than the UFG DL-BL sample in region II. In addition, the prepared UFG DL-BL maintained relatively stable  $\Theta$  in a wide strain region III, which was a prerequisite for effective tensile ductility [9,11,52]. At this stage, the work hardening rate of the uniform composite alternated between high and low with a large range due to the Mg solute clusters pinning dislocations. Compared to that of the uniform composite, the work hardening rate of the laminate composites alternated with a small range. This means that the dislocations in the DLs could slip easily.

The ex-situ TEM images (Fig. 7(c–f)) show the dislocations of the CG DL-BL laminate composite under different tensile strains. In the initial

stage of stretching, the DLs were more likely to start plastic deformation and some dislocations could be observed in the DLs rather than BLs at the elastic deformation stage (Fig. 7(c)). This also indicates that there was no obvious interaction between the CG DLs and the BLs at this stage.

After pre-stretching to 2% strain, some dislocations were observed at the DL edge near the interfaces (Fig. 7(d)). These results suggested that the geometrically necessary dislocations (GNDs) were formed due to the severe plastic deformation incongruity between DLs and BLs. With the further increase of strain, a large number of dislocations formed in the DLs, especially near the boundary between DL and BL (Fig. 7(e)). In the final stage of stretching, many dislocations could be observed even in the BLs (Fig. 7(f)). This indicates that the laminate structure could effectively increase the dislocation storage ability, thereby improving the ductility of the composites.

According to the above analysis, the tensile deformation for laminate composite could be divided into three stages. In the elastic stage, the DLs and BLs deformed independently (Fig. 7(g1)). In the elastic-plastic stage, plastic deformation occurred preferentially in the soft DLs, while the BLs were still in the elastic deformation stage (Fig. 7(g2)). In the plastic

stage, plastic deformation occurred in both the BLs and DLs (Fig. 7(g3)). However, because the plastic strain in the DLs was greater than that in the BLs, strain gradients occurred not only in the DLs but also in the BLs near the interfaces [53]. These strain gradients became larger as they continued to deform, thereby forming more GNDs and resulting in back stress hardening [53–55]. At different stages, the DLs and BLs bore different deformation. As the result, back stress and GNDs were generated to alleviate deformation incompatibility at the interface [54,55]. As reported [14,26,50], the laminate structure could provide substantial zone boundaries separating the different hardness zones. Therefore, the existence of the back stress between DLs and BLs improved the deformation ability of BLs, which was also the reason for the elongation increase of composites.

The fracture morphologies of laminate composites are shown in Fig. 8. Two phenomena could be observed. Firstly, the fracture surfaces for laminate composites were with a “V” shape rather than a straight line shape (Fig. 8(a) and (d)). This was because some micro-cracks occurred preferentially in different BLs, however, the existence of DLs was effective to delay crack growth and coalescence during deformation [30]. Secondly, many crack deflections could be observed on the fracture surface, which was experimentally supported by the presence of interlaminar cracks (Fig. 8(b), (c), (e), and (f)). It was reported that, at the last stage of deformation, the multiple microcracks could also contribute to elongation increase [56]. Ultimately, these events delay the onset of overall damage, allowing further inherent motion hardening and inducing additional ductility.

It should be mentioned that, the microstructure of laminate composites was quite different from that of other heterogeneous composites, such as bimodal composites [17,25,57]. In general, the best strength-ductility of the bimodal CNT/Al composites was achieved, as the DZs width was <math><10\ \mu\text{m}</math>. However, the same strength-ductility synergy could be achieved when the width of DLs in laminated composites was  $\sim 100\ \mu\text{m}$  [17,47]. That was to say, the morphologies of heterogeneous CNT/Al composite ductile zones had an important effect on mechanical properties.

#### 4.2. Effect of grain size in DL on the strength and ductility

The laminate composites consisted of continuous BL and DL, therefore, the strength of CG DL-BL and UFG DL-BL could be estimated as the rule of mixtures (ROM):

$$\sigma_L = \sigma_{BL} V_{BL} + \sigma_{DL} (1 - V_{BL}) \quad (1)$$

where  $V_{BL}$  is the volume fractions of brittle layers;  $\sigma_L$ ,  $\sigma_{BL}$  and  $\sigma_{DL}$  are the strengths of laminate composites, BL (3 vol% CNT/2009Al) and DL (2009Al), respectively. Eq. (1) indicates that higher strength of the DLs would lead to higher strength of the laminate composites. This means the finer grain size of DLs was beneficial to increasing the strength of the laminate composites, and this was why the YS of the UFG DL-BL was much larger than that of the CG DL-BL.

For the UFG DL-BL laminate composite, the volume fraction of the BLs was 0.66, while that of the CG DL-BL composite was 0.6. The calculated YS and UTS values for laminate composites were shown in Fig. 9(a) and (b). It can be seen that the calculated strength for the UFG DL-BL was very close to the experimental values, while the calculated strength for the CG DL-BL was underestimated. This indicates the extra strengthening for the CG DL-BL rather than the UFG DL-BL because the higher back stress would be induced for CG DL-BL with an obvious plastic deformation difference.

The SDP values of CG DL-BL and UFG DL-BL laminate composites calculated by ROM were 35 and 29 MJ/m<sup>3</sup>, respectively (Fig. 9(c)). For the UFG DL-BL laminate composite, the experimental value of SDP was very close to the ROM value, while that of CG DL-BL was obviously smaller than the ROM value.

There were two main reasons for the low elongation of CNT/Al composites. On one hand, CNTs greatly limited the plastic deformation of the Al matrix, which was a common phenomenon of discontinuously reinforced metal matrix composites [58]. On the other hand, the addition of CNTs significantly refined grain size and led to much lower dislocation storage capacity [17]. It was reported that, the excellent ductility for the laminate composites mainly stemmed from the plastic deformation of the DLs [16,17,52,59,60]. The addition of DLs could improve the dislocation storage capacity of composites, and thus improve the elongation of composites. In this study, the grain size of UFG DL-BL in DLs was smaller than that of CG DL-BL, but the elongations were the same. By refining the grains of DLs, both the strength and ductility of the laminate composites were improved.

Fig. 10 shows the TEM images of the UFG DL-BL at different stretching stages. On the whole, the dislocation accumulation trend of the UFG DL-BL under different strains was similar to that of the CG DL-BL (Fig. 7). Besides massive dislocations in DLs, there were also

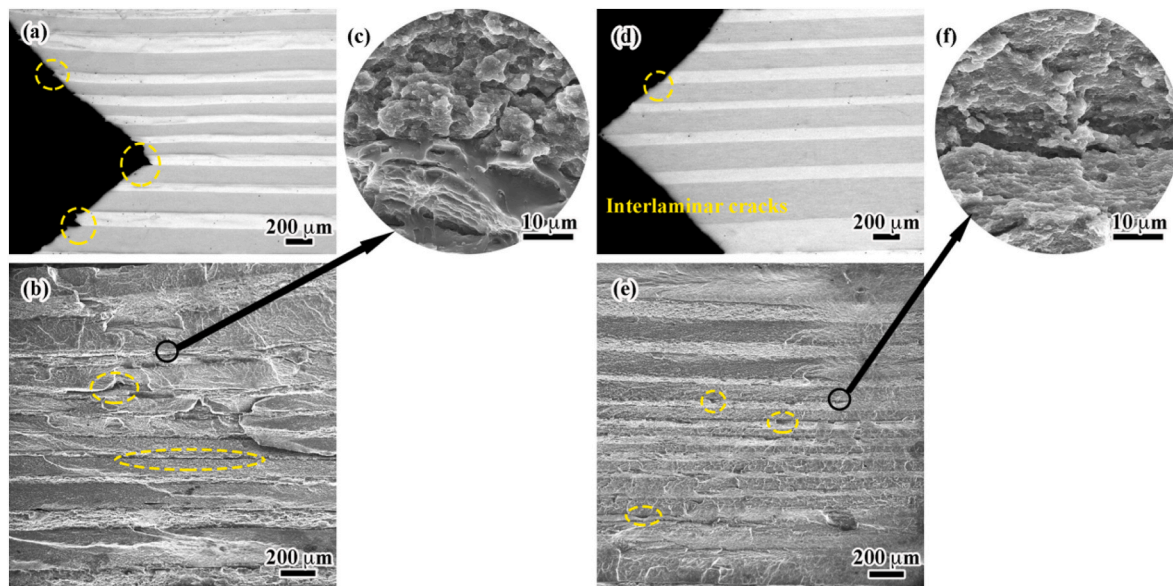


Fig. 8. Typical OM and SEM images of fracture surfaces of longitudinal section and cross-section for the two different laminate composites: (a) (b) (c) CG DL-BL. (d) (e) (f) UFG DL-BL.

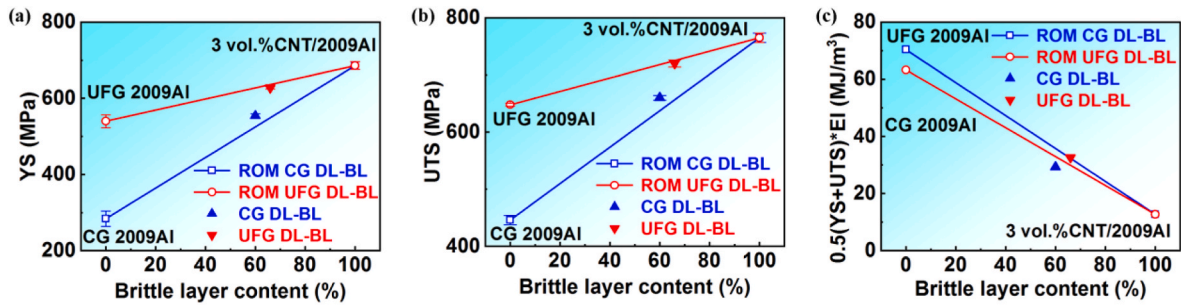


Fig. 9. Comparisons between experimental and calculated tensile properties of heterogeneous composites: (a) YS, (b) UTS, and (c) SDP.

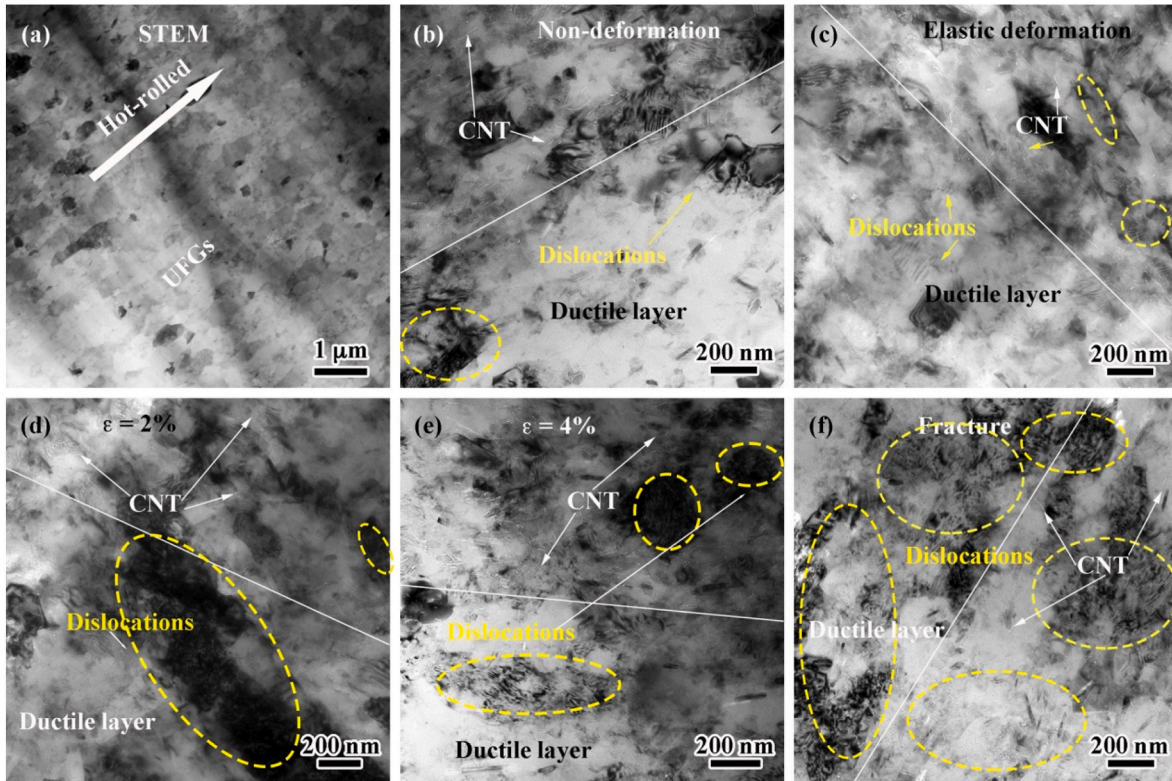


Fig. 10. Microstructure of UFG DL-BL laminate composite under different tensile stages with the increasing tensile strain. (a) and (b) non-deformation, (c) elastic stage, and (d) (f) plastic stage at different pre-stretching stages.

noticeable dislocations in BLs (Fig. 10(d)–(f)), which indicate that CNT/2009Al grains in the BLs could also plastically deform and sustain strain hardening in tension. This provided direct evidence that dislocations induced hardening and promote the observed high strain-hardening capability [61].

Overall, the grain size in the DLs had a significant effect on the ductility. On one hand, the larger grain size difference between DLs and BLs could lead to higher dislocation storage capacity and extra GND density, which were beneficial to higher ductility. On the other hand, the smaller grain size difference between DLs and BLs could result in more coordinated deformation between DLs and BLs. As a result, by properly refining the grain size in the BLs, the above two effects could be combined to obtain better strength and ductility. This could be well reflected in Fig. 9(c) that the calculated SDP of the UFG DL-BL was in accordance with the experimental result, while the calculated SDP of the CG DL-BL was overestimated as compared with that of the experimental result.

In general, the higher the content of the DLs, the better the ductility of composites [17,62]. However, in this study, the content of the DLs in

CG DL-BL was higher than that in UFG DL-BL, but the elongation was the same. Therefore, refining the grain size of the DL could improve the cooperative deformation ability of the DL and BL. At the same time, it could solve the problems of low yield strength and ultimate tensile strength of the CG DL-BL.

### 5. Conclusions

In this work, the CNT/2009Al composites with the laminate structure were prepared by combining the PM with hot-rolling. The main conclusions have been drawn:

- 1) CNT/2009Al laminate composites consisting of ductile layers free of CNTs and brittle layers rich in CNTs were successfully fabricated. The BLs and the DLs were densely bonded without defects, which was conducive to giving full play to the performance of each layer of the whole sample.
- 2) By constructing a laminate structure, the superior combination of strength and ductility of composites was successfully realized. The

increased dislocation storage ability and back-stress hardening effect induced by GNDs were the main reasons for excellent ductility for the laminate composites.

- 3) By properly refining the grain size of the BLs, the coordinated deformation capability between the DLs and BLs was improved. As a result, the UFG DL-BL obtains the synchronous improvement of strength and elongation, as compared with those of the uniform and CG DL-BL. This provided a new idea for the design of high strength-ductility composites.

#### Author statement

All authors contribute substantially to the paper. P. Y. Li (first author) carried out the data collection, data analysis and manuscript writing; X.N. Li fabricated the composites and tested the tensile properties; Z.Y. Liu designed the experiment and revised the manuscript; L.Q. Chen helped to revise the manuscript; B.L. Xiao participated in the design of the experiment and analysis of the experimental data; Z.Y. Ma revised the manuscript and provided the funding. All authors have read and approved the final manuscript.

#### Declaration of competing interest

The authors declare that they have no known competing financial interests or personal relationships that could have appeared to influence the work reported in this paper.

#### Data availability

Data will be made available on request.

#### Acknowledgment

This work was supported by: (a) the National Natural Science Foundation of China (No. 51931009, No. 52192595, No. 51871215, No.51871214); (b) the Liao Ning Revitalization Talents Program (No. XLYC1902058); (c) Shenyang young and middle-aged scientific and technological innovation talents support plan (No. RC210490); (d) the Youth Innovation Promotion Association CAS (No. 2020197).

#### References

- [1] Sadeghi B, Tan Z, Qi J, Li Z, Min X, Yue Z, et al. Enhanced mechanical properties of CNT/Al composite through tailoring grain interior/grain boundary affected zones. *Compos B Eng* 2021:223.
- [2] Ma K, Li XN, Liu K, Chen XG, Liu ZY, Xiao BL, et al. Improving the high-cycle fatigue strength of heterogeneous carbon nanotube/Al-Cu-Mg composites through grain size design in ductile-zones. *Compos B Eng* 2021:222.
- [3] Guo B, Song M, Zhang X, Liu Y, Cen X, Chen B, et al. Exploiting the synergic strengthening effects of stacking faults in carbon nanotubes reinforced aluminum matrix composites for enhanced mechanical properties. *Compos B Eng* 2021:211.
- [4] Zhang JF, Zhang XX, Andrá H, Wang QZ, Xiao BL, Ma ZY. A fast numerical method of introducing the strengthening effect of residual stress and strain to tensile behavior of metal matrix composites. *J Mater Sci Technol* 2021;87:167–75.
- [5] Qiu C, Su Y, Yang J, Wang X, Chen B, Ouyang Q, et al. Microstructural characteristics and mechanical behavior of SiC(CNT)/Al multiphase interfacial micro-zones via molecular dynamics simulations. *Compos B Eng* 2021:220.
- [6] Liu Q, Fan G, Tan Z, Guo Q, Xiong D, Su Y, et al. Reinforcement with intragranular dispersion of carbon nanotubes in aluminum matrix composites. *Compos B Eng* 2021:217.
- [7] Zhu SZ, Wang D, Xiao BL, Ma ZY. Effects of natural aging on precipitation behavior and hardening ability of peak artificially aged SiCp/Al-Mg-Si composites. *Compos B Eng* 2022:236.
- [8] Chen X, Tao J, Liu Y, Bao R, Li F, Li C, et al. Interface interaction and synergistic strengthening behavior in pure copper matrix composites reinforced with functionalized carbon nanotube-graphene hybrids. *Carbon* 2019;146:736–55.
- [9] Wang YM, Voisin T, McKeown JT, Ye J, Calta NP, Li Z, et al. Additively manufactured hierarchical stainless steels with high strength and ductility. *Nat Mater* 2018;17(1):63–71.
- [10] Ma E, Zhu T. Towards strength–ductility synergy through the design of heterogeneous nanostructures in metals. *Mater Today* 2017;20(6):323–31.
- [11] Lu K. Making strong nanomaterials ductile with gradients. *Science* 2014;345(6203):1455–6.
- [12] Meng X, Huang Y, Cao J, Shen J, dos Santos JF. Recent progress on control strategies for inherent issues in friction stir welding. *Prog Mater Sci* 2021;115.
- [13] Choi HJ, Shin JH, Bae DH. Grain size effect on the strengthening behavior of aluminum-based composites containing multi-walled carbon nanotubes. *Compos Sci Technol* 2011;71(15):1699–705.
- [14] Wu X, Yang M, Yuan F, Wu G, Wei Y, Huang X, et al. Heterogeneous lamella structure unites ultrafine-grain strength with coarse-grain ductility. *Proc Natl Acad Sci U.S.A* 2015;112(47):14501–5.
- [15] Du Y, Fan G, Yu T, Hansen N, Geng L, Huang X. Laminated Ti-Al composites: processing, structure and strength. *Mater Sci Eng* 2016;673:572–80.
- [16] Wang YF, Huang CX, He Q, Guo FJ, Wang MS, Song LY, et al. Heterostructure induced dispersive shear bands in heterostructured Cu. *Scripta Mater* 2019;170:76–80.
- [17] Liu ZY, Ma K, Fan GH, Zhao K, Zhang JF, Xiao BL, et al. Enhancement of the strength-ductility relationship for carbon nanotube/Al–Cu–Mg nanocomposites by material parameter optimisation. *Carbon* 2020;157:602–13.
- [18] Xu R, Tan Z, Fan G, Ji G, Xiong D-B, Guo Q, et al. High-strength CNT/Al-Zn-Mg-Cu composites with improved ductility achieved by flake powder metallurgy via elemental alloying. *Compos Appl Sci Manuf* 2018;111:1–11.
- [19] Liu X, Liu Z, Liu Y, Zafar Z, Lu Y, Wu X, et al. Achieving high strength and toughness by engineering 3D artificial nacre-like structures inTi6Al4V-Ti metallic composite. *Compos B Eng* 2022:230.
- [20] Zhang Z, Fan G, Tan Z, Zhao H, Xu Y, Xiong D, et al. Bioinspired multiscale Al<sub>2</sub>O<sub>3</sub>-rGO/Al laminated composites with superior mechanical properties. *Compos B Eng* 2021:217.
- [21] Liu M, Zhang C, Meng Z, Zhao G, Chen L. Atomic diffusion mechanism and interface nanomechanics in the Al/Ti composite structures. *Compos B Eng* 2022:230.
- [22] Wang Y, Li X. 4D-printed bi-material composite laminate for manufacturing reversible shape-change structures. *Compos B Eng* 2021:219.
- [23] Chen B, Shen J, Ye X, Jia L, Li S, Umeda J, et al. Length effect of carbon nanotubes on the strengthening mechanisms in metal matrix composites. *Acta Mater* 2017;140:317–25.
- [24] Kümmel F, Hausöl T, Höppel HW, Göken M. Enhanced fatigue lives in AA1050A/AA5005 laminated metal composites produced by accumulative roll bonding. *Acta Mater* 2016;120:150–8.
- [25] Chen W, He W, Chen Z, Jiang B, Liu Q. Extraordinary room temperature tensile ductility of laminated Ti/Al composite: roles of anisotropy and strain rate sensitivity. *Int J Plast* 2020:133.
- [26] Bhattacharjee T, Wani IS, Sheikh S, Clark IT, Okawa T, Guo S, et al. Simultaneous strength-ductility enhancement of a nano-lamellar AlCoCrFeNi<sub>2.1</sub> eutectic high entropy alloy by cryo-rolling and annealing. *Sci Rep* 2018;8(1):3276.
- [27] Yang M, Yan D, Yuan F, Jiang P, Ma E, Wu X. Dynamically reinforced heterogeneous grain structure prolongs ductility in a medium-entropy alloy with gigapascal yield strength. *Proc Natl Acad Sci U.S.A* 2018;115(28):7224–9.
- [28] Wang H, Zhu C, Vecchio KS. Deformation and fracture evolution of FeAl-based metallic-intermetallic laminate (MIL) composites. *Acta Mater* 2020;194:496–515.
- [29] Wu H, Fan G, Jin BC, Geng L, Cui X, Huang M. Fabrication and mechanical properties of TiBw/Ti-Ti(Al) laminated composites. *Mater Des* 2016;89:697–702.
- [30] Wu H, Fan G, Huang M, Geng L, Cui X, Xie H. Deformation behavior of brittle/ductile multilayered composites under interface constraint effect. *Int J Plast* 2017;89:96–109.
- [31] Yang LW, Mayer C, Chawla N, Llorca J, Molina-Aldareguia JM. Deformation mechanisms of ultra-thin Al layers in Al/SiC nanolaminates as a function of thickness and temperature. *Phil Mag* 2016;96(32–34):3336–55.
- [32] Ferraro C, Meille S, Réthoré J, Ni N, Chevalier J, Saiz E. Strong and tough metal/ceramic micro-laminates. *Acta Mater* 2018;144:202–15.
- [33] Huang M, Xu C, Fan G, Maawad E, Gan W, Geng L, et al. Role of layered structure in ductility improvement of layered Ti-Al metal composite. *Acta Mater* 2018;153:235–49.
- [34] Liu ZY, Xiao BL, Wang WG, Ma ZY. Developing high-performance aluminum matrix composites with directionally aligned carbon nanotubes by combining friction stir processing and subsequent rolling. *Carbon* 2013;62:35–42.
- [35] Chen B, Jia L, Li S, Imai H, Takahashi M, Kondoh K. In situ synthesized Al<sub>4</sub>C<sub>3</sub>Nanorods with excellent strengthening effect in aluminum matrix composites. *Adv Eng Mater* 2014;16(8):972–5.
- [36] Zhou W, Bang S, Kurita H, Miyazaki T, Fan Y, Kawasaki A. Interface and interfacial reactions in multi-walled carbon nanotube-reinforced aluminum matrix composites. *Carbon* 2016;96:919–28.
- [37] Chen B, Shen J, Ye X, Imai H, Umeda J, Takahashi M, et al. Solid-state interfacial reaction and load transfer efficiency in carbon nanotubes (CNTs)-reinforced aluminum matrix composites. *Carbon* 2017;114:198–208.
- [38] Xie Y, Meng X, Chang Y, Mao D, Yang Y, Xu Y, et al. Ameliorating strength-ductility efficiency of graphene nanoplatelet-reinforced aluminum composites via deformation-driven metallurgy. *Compos Sci Technol* 2022:219.
- [39] Xie Y, Meng X, Li Y, Mao D, Wan L, Huang Y. Insight into ultra-refined grains of aluminum matrix composites via deformation-driven metallurgy. *Compos Commun* 2021:26.
- [40] Choi H, Shin J, Min B, Park J, Bae D. Reinforcing effects of carbon nanotubes in structural aluminum matrix nanocomposites. *J Mater Res* 2011;24(8):2610–6.
- [41] Esawi AMK, Morsi K, Sayed A, Taher M, Lanka S. The influence of carbon nanotube (CNT) morphology and diameter on the processing and properties of CNT-reinforced aluminum composites. *Compos Appl Sci Manuf* 2011;42(3):234–43.
- [42] Stein J, Lenczowski B, Anglaret E, Fréty N. Influence of the concentration and nature of carbon nanotubes on the mechanical properties of AA5083 aluminium alloy matrix composites. *Carbon* 2014;77:44–52.

- [43] Liu ZY, Zhao K, Xiao BL, Wang WG, Ma ZY. Fabrication of CNT/Al composites with low damage to CNTs by a novel solution-assisted wet mixing combined with powder metallurgy processing. *Mater Des* 2016;97:424–30.
- [44] Liu ZY, Xiao BL, Wang WG, Ma ZY. Modelling of carbon nanotube dispersion and strengthening mechanisms in Al matrix composites prepared by high energy ball milling-powder metallurgy method. *Compos Appl Sci Manuf* 2017;94:189–98.
- [45] Xu R, Tan Z, Xiong D, Fan G, Guo Q, Zhang J, et al. Balanced strength and ductility in CNT/Al composites achieved by flake powder metallurgy via shift-speed ball milling. *Compos Appl Sci Manuf* 2017;96:57–66.
- [46] Liu ZY, Xiao BL, Wang WG, Ma ZY. Tensile strength and electrical conductivity of carbon nanotube reinforced aluminum matrix composites fabricated by powder metallurgy combined with friction stir processing. *J Mater Sci Technol* 2014;30(7): 649–55.
- [47] Fu X, Tan Z, Ma Z, Li Z, Fan G, Xiong D-B, et al. Powder assembly & alloying to CNT/Al–Cu–Mg composites with trimodal grain structure and strength-ductility synergy. *Compos B Eng* 2021:225.
- [48] Wegst UG, Bai H, Saiz E, Tomsia AP, Ritchie RO. Bioinspired structural materials. *Nat Mater* 2015;14(1):23–36.
- [49] Zhang C, Zhu C, Vecchio K. Non-equiatom FeNiCoAl-based high entropy alloys with multiscale heterogeneous lamella structure for strength and ductility. *Mater Sci Eng* 2019;743:361–71.
- [50] Yang MX, Yuan FP, Xie QG, Wang YD, Ma E, Wu XL. Strain hardening in Fe–16Mn–10Al–0.86C–5Ni high specific strength steel. *Acta Mater* 2016;109: 213–22.
- [51] Yang M, Pan Y, Yuan F, Zhu Y, Wu X. Back stress strengthening and strain hardening in gradient structure. *Materials Research Letters* 2016;4(3):145–51.
- [52] Wang Y, Chen M, Zhou F, Ma E. High tensile ductility in a nanostructured metal. *Nature* 2002;419:912–5.
- [53] Wu X, Zhu Y. Heterogeneous materials: a new class of materials with unprecedented mechanical properties. *Materials Research Letters* 2017;5(8): 527–32.
- [54] Nie J, Chen Y, Chen X, Liu X, Liu G, Zhao Y, et al. Stiff, strong and ductile heterostructured aluminum composites reinforced with oriented nanoplatelets. *Scripta Mater* 2020;189:140–4.
- [55] Chen Y, Nie J, Wang F, Yang H, Wu C, Liu X, et al. Revealing hetero-deformation induced (HDI) stress strengthening effect in laminated Al-(TiB<sub>2</sub>+TiC)<sub>p</sub>/6063 composites prepared by accumulative roll bonding. *J Alloys Compd* 2020:815.
- [56] Huang LJ, Geng L, Peng HX. Microstructurally inhomogeneous composites: is a homogeneous reinforcement distribution optimal? *Prog Mater Sci* 2015;71: 93–168.
- [57] Sun H, Saba F, Fan G, Tan Z, Li Z. Micro/nano-reinforcements in bimodal-grained matrix: a heterostructure strategy for toughening particulate reinforced metal matrix composites. *Scripta Mater* 2022:217.
- [58] Torralba JM, da Costa CE, Velasco F. PM aluminum matrix composites an overview. *J Mater Process Technol* 2003;133:203–6.
- [59] Zhu L, Shi S, Lu K, Lu J. A statistical model for predicting the mechanical properties of nanostructured metals with bimodal grain size distribution. *Acta Mater* 2012;60 (16):5762–72.
- [60] Ma K, Liu ZY, Liu K, Chen XG, Xiao BL, Ma ZY. Structure optimization for improving the strength and ductility of heterogeneous carbon nanotube/Al–Cu–Mg composites. *Carbon* 2021;178:190–201.
- [61] Shi P, Ren W, Zheng T, Ren Z, Hou X, Peng J, et al. Enhanced strength-ductility synergy in ultrafine-grained eutectic high-entropy alloys by inheriting microstructural lamellae. *Nat Commun* 2019;10(1):489.
- [62] Fu X, Tan Z, Min X, Li Z, Yue Z, Fan G, et al. Trimodal grain structure enables high-strength CNT/Al–Cu–Mg composites higher ductility by powder assembly & alloying. *Materials Research Letters* 2020;9(1):50–7.